

GENERAL RELATIVISTIC MAGNETOHYDRODYNAMIC SIMULATIONS OF JETS FROM BLACK HOLE ACCRETION DISKS: TWO-COMPONENT JETS DRIVEN BY NONSTEADY ACCRETION OF MAGNETIZED DISKS

SHINJI KOIDE

Faculty of Engineering, Toyama University, Gofuku, Toyama 930, Japan

AND

KAZUNARI SHIBATA AND TAKAHIRO KUDOH

National Astronomical Observatory, Mitaka-shi, Tokyo 181, Japan

Received 1997 July 7; accepted 1997 November 19; published 1998 February 13

ABSTRACT

The radio observations have revealed the compelling evidence of the existence of relativistic jets not only from active galactic nuclei but also from “microquasars” in our Galaxy. In the cores of these objects, it is believed that a black hole exists and that violent phenomena occur in the black hole magnetosphere, forming the relativistic jets. To simulate the jet formation in the magnetosphere, we have newly developed the general relativistic magnetohydrodynamic code. Using the code, we present a model of these relativistic jets, in which magnetic fields penetrating the accretion disk around a black hole play a fundamental role of inducing nonsteady accretion and ejection of plasmas. According to our simulations, a jet is ejected from a close vicinity to a black hole (inside $3r_s$, where r_s is the Schwarzschild radius) at a maximum speed of $\sim 90\%$ of the light velocity (i.e., a Lorentz factor of ~ 2). The jet has a *two-layered shell structure* consisting of a fast *gas pressure-driven jet* in the inner part and a slow *magnetically driven jet* in the outer part, both of which are collimated by the global poloidal magnetic field penetrating the disk. The former jet is a result of a strong pressure increase due to *shock formation* in the disk through fast accretion flow (“advection-dominated disk”) inside $3r_s$, which has never been seen in the nonrelativistic calculations.

Subject headings: accretion, accretion disks — black hole physics — galaxies: jets — magnetic field — methods: numerical — MHD — relativity

1. INTRODUCTION

The radio jets ejected from active galactic nuclei (AGNs) sometimes show proper motion with apparent velocity exceeding the speed of light (Pearson et al. 1981; Hughes 1991). This phenomenon, called the superluminal motion, is explained as relativistic jets propagating in a direction almost toward us with a Lorentz factor greater than 2 (Rees 1966) and has been thought to be ejected from close vicinity of hypothetical supermassive black holes powering AGNs (Linden-Bell 1969; Rees 1984). Recently, similar superluminal motion has been discovered in some compact radio/X-ray sources (i.e., “microquasars”) in our Galaxy such as GRS 1915+105 and GRO J1655–40 (Mirabel & Rodriguez 1994; Tingay et al. 1995), which are considered to be black hole candidates. In spite of the vast difference in the luminosity and the size of “microquasars” in our Galaxy (e.g., GRS 1915+105, whose luminosity is 3×10^{38} ergs s^{-1} and the size less than 10^6 cm) and those of AGNs (whose luminosity is $\sim 10^{47}$ ergs s^{-1} and the size less than 10^{14} cm), both objects are believed to be powered by gravitational energy released during accretion of plasmas onto black holes. (The mass of black holes M_{BH} is estimated to be less than $10 M_{\odot}$ for microquasars and $\sim 10^8 M_{\odot}$ for AGNs. If we normalize the length by the Schwarzschild radius $r_s = 2GM_{\text{BH}}/c^2$, where G is the gravitational constant and c is the speed of light, both objects become similar and thus can be understood in a unified model, as in the following.)

Since accreting plasmas have nonzero angular momentum, they form an accretion disk orbiting around a black hole. Similarly, if accreting plasmas have nonzero poloidal magnetic flux, magnetic flux accumulates in the inner region of the accretion disk to form global poloidal magnetic fields penetrating the disk. Such poloidal fields could also be generated by the dynamo action inside the accretion disk. In either case, poloidal

fields are twisted by the rotating disk to the azimuthal direction, and this process extracts angular momentum from the disk, enabling efficient accretion of disk plasmas onto black holes. On the other hand, the magnetic twist generated during this process accelerates plasmas in the surface layer of the disk toward both polar directions by the $\mathbf{J} \times \mathbf{B}$ force, and the accelerated plasmas form bipolar relativistic jets that are also collimated by the magnetic force. This magnetic mechanism has been proposed not only for AGN jets (Lovelace 1976; Blandford & Payne 1982; Pelletier et al. 1996; Meier et al. 1997) but also for protostellar jets (Pudritz & Norman 1986; Uchida & Shibata 1985; Shibata & Uchida 1986; Ouyed, Pudritz, & Stone 1997). Theories of the steady relativistic flow in the black hole magnetosphere have been developed with the assumption of fixed poloidal magnetic field configurations (Camenzind 1986; Takahashi et al. 1990), asymptotic aspects (Begelman & Li 1994; Tomimatsu 1994), a force-free magnetic field (Okamoto 1992), or self-similar solutions (Li, Chiueh, & Begelman 1992). As for the full relativistic magnetohydrodynamics (without these assumptions), numerical simulations have been used to study the jet propagation through magnetic fields within the special relativistic framework (Koide, Nishikawa, & Mutel 1996; van Putten 1996; Koide 1997; Nishikawa et al. 1997). Hawley & Smarr (1986) performed general relativistic (nonmagnetic) hydrodynamic simulations of the jet formation near a black hole, while Yokosawa (1993) carried out general relativistic magnetohydrodynamic simulations of accretion onto a rotating black hole. However, no one has yet performed full general relativistic magnetohydrodynamic (GRMHD) numerical simulations on the *formation of jets near a black hole*.

In this Letter, we report on the first full GRMHD numerical simulation of magnetically driven relativistic jets from an ac-

cretion disk around a black hole, by extending a previous non-steady Newtonian magnetohydrodynamic (MHD) jet model (Uchida & Shibata 1985; Shibata & Uchida 1986) to a general relativistic regime. We have developed a GRMHD code using the simplified total variation diminishing (TVD) method.

It must be noted here that observations of superluminal jet sources revealed that these jets are ejected intermittently in association with flares in compact sources (Hughes 1991; Mirabel & Rodriguez 1994). It has also been theoretically argued that accretion disks near black holes can evolve into advection-dominated disks that have large radial accretion flows with possible time dependence or instability (Abramowicz 1996; Kato, Abramowicz, & Chen 1996; Balbus & Hawley 1991). Hence, the time-dependent approach (as in this Letter) is essential, even though some basic physics can be understood by steady models (Kudoh & Shibata 1995, 1997).

2. NUMERICAL METHOD

We use a $3 + 1$ formalism of general relativistic conservation laws of particle number, momentum, and energy and Maxwell equations with infinite electric conductivity (Thorne, Price, & MacDonald 1986; Koide et al. 1996; Koide 1997; Nishikawa et al. 1997; Koide, Shibata, & Kudoh 1998). When we take the nonrelativistic limit of these equations ($c \rightarrow \infty$), they reduce to Newtonian MHD equations. Therefore, these equations are called GRMHD equations. The Schwarzschild metric, which provides the spacetime around the black hole at rest, is used in the calculation. It is noted that the GRMHD equations with the metric are identical to the special relativistic equations on the general coordinates, except for the gravitational force terms and the geometric factor of the lapse function. This means it is not so difficult to develop the GRMHD code from the special relativistic one (Koide et al. 1996; Koide 1997; Nishikawa et al. 1997). The simulation is performed in the region $1.05r_s \leq r \leq 20r_s$, $0 \leq \theta \leq \pi/2$, with 210×70 meshes, assuming the axisymmetry with respect to the z -axis and the mirror symmetry with respect to the plane $z = 0$. Here r and θ are radial and polar coordinates of the spherical coordinates, respectively. The radiative boundary condition is employed at $r = 1.05r_s$ and $r = 20r_s$. In the simulations, we use the modified *tortoise* coordinates, $x \equiv \ln(r/r_s - 1)$ (Press 1971). To avoid the numerical oscillation, we use the simplified TVD method (Davis 1984; Koide et al. 1996; Koide 1997). This method is useful because we do not have to solve the eigenvalue problem of the Jacobian of the GRMHD equations while it is monotonicity preserving. We checked this GRMHD code by the steady free-fall flow, Keplerian motion, and MHD shock waves around a black hole (Koide et al. 1998).

3. RESULTS

Figure 1 (Plate L8) shows the time development of the relativistic jet formation in the black hole magnetosphere. These figures show the rest mass density (*blue and white*), velocity (*vector*), and magnetic field (*solid lines*) in $-7r_s \leq x \leq 7r_s$, $-7r_s \leq z \leq 7r_s$. The black circles at the centers show the black hole inside the event horizon at Schwarzschild radius r_s . The initial state in the simulation consists of a hot corona around the black hole and a cold accretion disk (Fig. 1a). In the corona, plasmas are assumed to be isothermal and in hydrostatic equilibrium, where the proper sound velocity is constant ($v_s = 0.53c$). The accretion disk is located at $|\cot \theta| \leq 0.125$, $r \geq r_d = 3r_s$ and is rotating around the black hole with Keplerian velocity $v_K = c/[2(r/r_s - 1)]^{1/2}$. In this case, the rotational velocity of the disk is 50% of the light velocity at its inner edge

($r = 3r_s$, $z = 0$). The mass density of the disk is 400 times that of the corona. In addition, the magnetic field crosses the accretion disk perpendicularly. We use the Wald solution, which provides the uniform magnetic field around the black hole (Wald 1974). At the inner edge of the accretion disk, the proper Alfvén velocity is $v_{A,\text{disk}} = 0.015c$ [note that $v_{A,\text{corona}}(r = 3r_s) = 0.3c$ and plasma beta, $\beta(r = 3r_s) \equiv p_{\text{gas}}/p_{\text{mag}} \sim 3.7$ in the corona and the disk].

Figure 1b shows the snapshot at $t = 10\tau_s$, when the disk rotates a quarter cycle, where τ_s is defined as $\tau_s \equiv r_s/c$. The Alfvén wave propagates along the magnetic field lines from the disk, and the front of the wave reaches $z \sim 5.5r_s$ at this stage. The accretion disk loses its angular momentum as a result of magnetic braking and begins to fall toward the black hole, as shown in the vector plot of Figure 1b.

At $t = 40\tau_s$, a jet starts to be ejected at the inner edge of the accretion disk around $x \sim 1.7r_s$, $z \sim 0.5r_s$ (Fig. 1c). At this time, the disk rotates almost one cycle and penetrates into the unstable region ($r \leq 3r_s$). The plasma in the unstable region begins to fall into the black hole rapidly and collides with the high-pressure corona near the black hole. The magnetic flux tubes and the plasma are compressed by this strong collision. Figure 1d shows the final stage of this simulation at $t = 91\tau_s$ when the accretion disk rotates more than two cycles around the black hole. The jet is formed almost along the global poloidal magnetic field lines. The jet is ejected from $x \sim 1.5r_s$, $z \sim 0$. The maximum poloidal component of the jet velocity is $0.88c$, which corresponds to a Lorentz factor of 2.1 at $x \sim 3.0r_s$, $z \sim 3.5r_s$. It is remarkable that magnetic field lines are highly stretched and deformed by the jet. This figure also shows that the jet has a two-layered structure, consisting of the inner fast jet and the outer slow jet (see also Fig. 2 [Pl. L9] for an enlargement of the region near a black hole).

What is the acceleration mechanism of the inner and outer jets? Figure 3 (Plate L10) shows the distributions of several physical quantities around the jets, revealing that the inner jet is accelerated by the gas pressure force while the outer jet is accelerated by the electromagnetic force (Fig. 3d). The outer jet is physically the same as the magnetically driven jet in a Newtonian MHD simulation model such as that of Shibata & Uchida (1986), and hence it is called a *magnetically driven jet*. In this jet, the toroidal component of the magnetic field (B_ϕ) is larger than the vertical component (B_z) (Fig. 3e), and the magnetic pressure dominates the gas pressure [i.e., low $\beta(<1)$ plasma] (Fig. 3c). Figure 3a shows that the outer jet is located between the high rotation velocity regions, which means it is caused by the energy release of the rotation velocity. These characteristics are similar to those seen in Newtonian magnetically driven jets. On the other hand, the inner fast jet is called a *gas pressure-driven jet* and is an entirely new feature that has never been found in corresponding Newtonian MHD simulations (see Fig. 4 [Pl. L11]). In the inner jet, the toroidal field (B_ϕ) is much smaller than that in the outer jet (Fig. 3e), and the gas pressure dominates the magnetic pressure [i.e., high $\beta(>1)$ plasma] (Fig. 3c). In fact, the temperature of the inner fast jet is high while that of the outer slow jet is low (Fig. 3b). The rotational velocity is smaller than that in the outer jet (Fig. 3f).

The inner jet rapidly reaches the relativistic speed within a small distance (the maximum poloidal component of the jet velocity is $0.88c$, and the acceleration distance is only several r_s). This rapid acceleration is a result of rapid pressure increase due to a shock, which is formed inside the rapidly infalling disk (i.e., “advection-dominated disk”) induced by the strong gravity of the black hole below the last stable Keplerian orbit

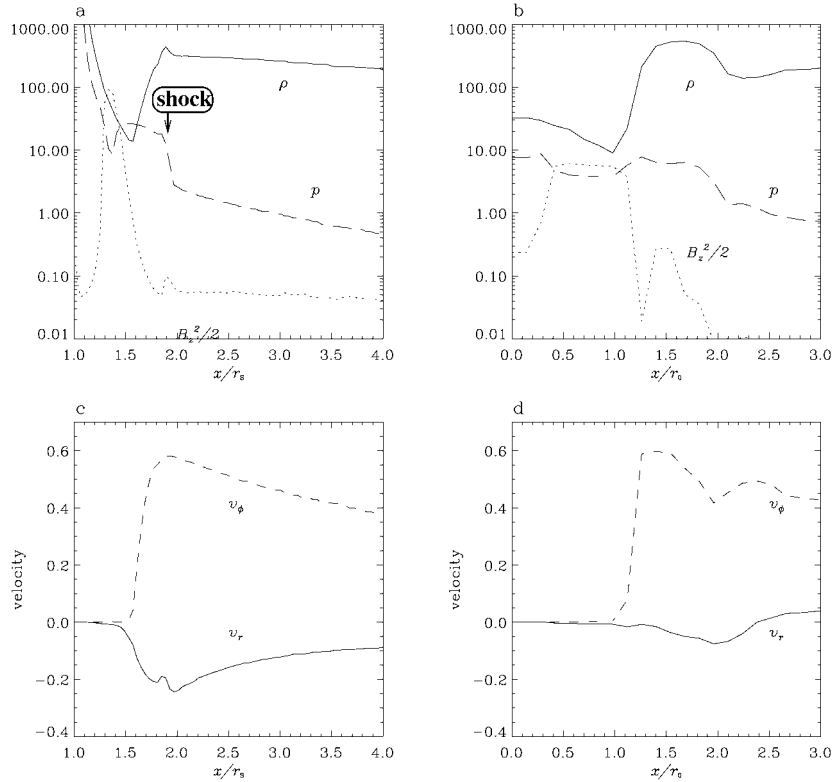


FIG. 5.—The physical variables at the equator for the (a, c) relativistic case and the (b, d) nonrelativistic case at $t = 91\tau_s$ and $t = 100\tau_0$, respectively. (a, b) The proper mass density ρ , proper pressure p , and magnetic pressure $B_z^2/2$; (c, d) the accretion velocity v_r and the azimuthal velocity v_ϕ . In the relativistic case, the accretion disk inside the last Keplerian stable orbit falls into the black hole rapidly. The reverse shock wave is induced in the accretion disk at $r = 1.95r_s$. In the downstream, the extreme high pressure region is formed and causes the relativistic jet with the collimation of the magnetic field. In the nonrelativistic case, we do not find such strong shock structure. Only the magnetically driven jet would be channeled.

at $r = 3r_s$. Figure 5 shows one-dimensional spatial distribution of physical quantities along the equatorial plane of the disk for both the relativistic and nonrelativistic cases. In the relativistic case, the accretion disk (high-density region) falls into the black hole rapidly, and its edge reaches near $r \sim 1.7r_s$ (Fig. 5a). The accretion velocity v_r is as large as half of the azimuthal velocity v_ϕ because the disk plasma is in the unstable region of the Keplerian motion (Fig. 5c). A shock (a kind of a reverse shock or a Mach disk) is formed inside the rapidly falling disk, so that the gas pressure behind the shock is increased very much in order to accelerate the disk plasma to both polar directions along global poloidal magnetic fields. Similar shock and jet formation structure is found by Hawley & Smarr (1986) using general relativistic hydrodynamic simulations. On the other hand, in the nonrelativistic case, the accretion velocity is much smaller than the azimuthal velocity (Fig. 5d). In this case, the strength of the shock in the disk is much smaller than that of the relativistic case so that the gas pressure increase behind the shock is weak (Fig. 5b). Consequently, only the magnetically driven jet is formed in this case.

Figure 6 illustrates the physical processes revealed by our general relativistic MHD simulations of jets ejected from magnetized accretion disks near a black hole.

4. DISCUSSION

To investigate the dependence of the jet velocity on the initial magnetic field B_0 , we performed simulations of the nine cases with different B_0 ($B_0/\rho_0 c^2 = 0, 0.15, 0.20, 0.25, 0.3, 0.35, 0.4, 0.5, \text{ and } 1.0$, where ρ_0 is the initial mass density of the corona at $r = 3r_s$). The maximum velocity of the magnetically driven

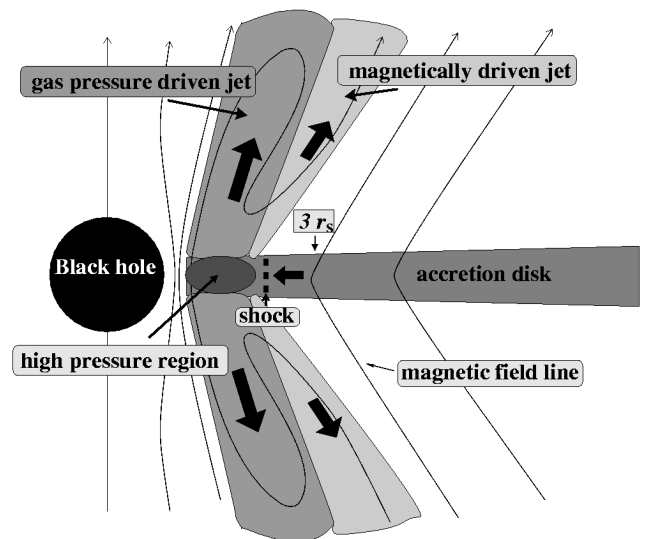


FIG. 6.—Schematic picture of the jet formation from the accretion disk around the black hole. Below the last stable orbit of Keplerian motion $r = 3r_s$, the accretion disk fall into the hole rapidly. The reverse shock is formed in the rapidly falling disk. The relativistic jet is formed by the extremely high pressure behind the shock front (gas pressure–driven jet). The magnetically driven jet is formed in the outer layer of the gas pressure–driven jet.

jet increases as the initial magnetic field increases, $v_{\text{jet}} \propto B^a$, where $a \sim 0.5\text{--}0.8$, which is similar to the relation known for the magnetically driven steady jets (Kudoh & Shibata 1995, 1997). On the other hand, the velocity of the gas pressure-driven jet has no monotonic dependence on the initial magnetic field. The velocity increases as the initial magnetic field increases until the value $B_0 = 0.4\rho_0 c^2$. This is true for the following reason: when the initial magnetic field is stronger, the disk loses the angular momentum more rapidly and the disk falls toward the black hole faster. The gas pressure in the shocked region by the falling disk is larger, and the gas pressure-driven jet becomes faster. When the field is larger than the critical value, the velocity decreases as the field increases. This is explained by the magnetic dragging against the jet propagation, i.e., by the deceleration $\mathbf{J} \times \mathbf{B}$ force due to highly deformed magnetic field lines as seen in Figure 1d.

It should be noted, however, that the formation of the gas pressure-driven jet may depend on the physical condition of the corona, such as the initial gas pressure distribution. In our model, the initial coronal plasma is assumed to be in hydrostatic equilibrium, so that the gas pressure near a black hole is very high. This might affect the result. In order to check this, we studied several cases in which the initial coronal plasma is not in hydrostatic equilibrium but in a free-fall state. We found that the gas pressure-driven jet is produced even in such cases if the initial coronal temperature is the same as that assumed in this Letter. The results in these cases will be reported elsewhere.

According to Mirabel & Rodriguez (1995), the velocity of the ejecta from black hole candidates such as *microquasars* GRS 1915+105 and GRO J1655-40 is larger than $0.9c$, whereas it is $\leq 0.3c$ in neutron star candidates in our Galaxy such as Cygnus X-3, SS 433, and the Crab pulsar. Our simulations explain these observations as follows. The unstable orbit region exists around the black hole, and the gas

pressure-driven jet is formed in such a region according to our results. The jet has very low density and could reach to the relativistic regime. This situation may correspond to the case of GRS 1915+105 and GRO J1655-40. On the other hand, around the neutron star, which should correspond to the cores of SS 433 and Cygnus X-3, such an unstable orbit region never appears. In such case, only the magnetically driven jet is permitted. The jet has high-mass density and is limited to the slow terminal velocity, i.e., the subrelativistic one.

The transient properties of the gas pressure-driven jet may also explain some of observations, e.g., the transient ejecta may correspond to the knot, which is frequently observed in extragalactic jets and microquasars. It is conjectured that the knot is surrounded by the steady outer-layer-shell jet. Recently, the observations with the *Hubble Space Telescope*, ground-based optical telescopes, and the Very Large Array show that the optical emission is everywhere interior to the radio emission or, in other words, is more localized toward the axis of the jets of M87 (Sparks, Biretta, & Macchetto 1996) and 3C 273 (Thomson, MacKay, & Wright 1993). This observational aspect may be explained by our results. That is, the optical knot corresponds to the gas pressure-driven jet, whose magnetic field strength is small, and the radio outer jet to the magnetically driven jet, which is strongly magnetized and emits the radio waves.

We thank M. Inda-Koide for her discussions and important comments for this study. We also thank M. Takahashi, T. Yokoyama, K. Hirotani, K.-I. Nishikawa, J.-I. Sakai, and R. L. Mutel for their discussions and encouragement, and we also thank the National Institute for Fusion Science and the National Astronomical Observatory for the use of supercomputers. This work is partially supported by Sumitomo Foundation.

REFERENCES

- Abramowicz, M. 1996, in *Physics of Accretion Disks*, ed. S. Kato et al. (Amsterdam: Overseas Publishers Association), 1
- Balbus, S. A., & Hawley, J. F. 1991, *ApJ*, 376, 214
- Begelman, M. C., & Li, Z.-Y. 1994, *ApJ*, 426, 269
- Blandford, R. D., & Payne, D. G. 1982, *MNRAS*, 199, 883
- Camenzind, M. 1986, *A&A*, 156, 137
- Davis, S. F. 1984, NASA Contractor Rep. 172373, ICASE Rep. 84-20
- Hawley, J. F., & Smarr, L. L. 1986, in *AIP Conf. Proc. 144, Magnetospheric Phenomena in Astrophysics*, ed. R. I. Epstein (New York: AIP), 263
- Hughes, P. A., ed. 1991, *Beams and Jets in Astrophysics* (New York: Cambridge Univ. Press)
- Kato, S., Abramowicz, M., & Chen, X. 1996, *PASJ*, 48, 67
- Koide, S. 1997, *ApJ*, 478, 66
- Koide, S., Nishikawa, K.-I., & Mutel, R. L. 1996, *ApJ*, 463, L71
- Koide, S., Shibata, K., & Kudoh, T. 1998, in preparation
- Kudoh, T., & Shibata, K. 1995, *ApJ*, 452, L41
- . 1997, *ApJ*, 474, 362
- Li, Z.-Y., Chiueh, T., & Begelman, M. C. 1992, *ApJ*, 394, 459
- Linden-Bell, D. 1969, *Nature*, 223, 690
- Lovelace, R. V. E. 1976, *Nature*, 262, 649
- Meier, D. L., Edgington, S., Godon, P., Payne, D. G., & Lind, K. R. 1997, *Nature*, 388, 350
- Mirabel, I. F., & Rodriguez, L. F. 1994, *Nature*, 371, 46
- . 1995, in *Ann. NY Acad. Sci.*, 759, 17th Texas Symp. on Relativistic Astrophysics and Cosmology, ed. H. Böhringer & J. Trümper, 21
- Nishikawa, K.-I., Koide, S., Sakai, J.-I., Christodoulou, D. M., Mutel, R. L., & Sol, H. 1997, *ApJ*, 483, L45
- Okamoto, I. 1992, *MNRAS*, 254, 192
- Ouyed, R., Pudritz, R. E., & Stone, J. M. 1997, *Nature*, 385, 409
- Pearson, J. J., et al. 1981, *Nature*, 290, 365
- Pelletier, G., Ferreira, J., Henri, G., & Marcowith, A. 1996, in *Solar and Astrophysical Magnetohydrodynamic Flows*, ed. K. C. Tsinganos (Dordrecht: Kluwer), 643
- Press, W. H. 1971, *ApJ*, 170, L105
- Pudritz, R. E., & Norman, C. 1986, *ApJ*, 301, 571
- Rees, M. J. 1966, *Nature*, 211, 468
- . 1984, *ARA&A*, 22, 471
- Shibata, K., & Uchida, Y. 1986, *PASJ*, 38, 631
- Sparks, W. B., Biretta, J. A., & Macchetto, F. 1996, *ApJ*, 473, 254
- Takahashi, M., Nitta, S., Tatematsu, Y., & Tomimatsu, A. 1990, *ApJ*, 363, 206
- Thomson, R. C., MacKay, C. D., & Wright, A. E. 1993, *Nature*, 365, 133
- Thorne, K. S., Price, R. H., & MacDonald, D. A. 1986, *Black Holes: The Membrane Paradigm* (New Haven: Yale Univ. Press)
- Tingay, S. J., et al. 1995, *Nature*, 374, 141
- Tomimatsu, A. 1994, *PASJ*, 46, 123
- Uchida, Y., & Shibata, K. 1985, *PASJ*, 37, 515
- van Putten, M. H. P. M. 1996, *ApJ*, 467, L57
- Wald, R. M. 1974, *Phys. Rev. D*, 10, 1680
- Yokosawa, M. 1993, *PASJ*, 45, 207

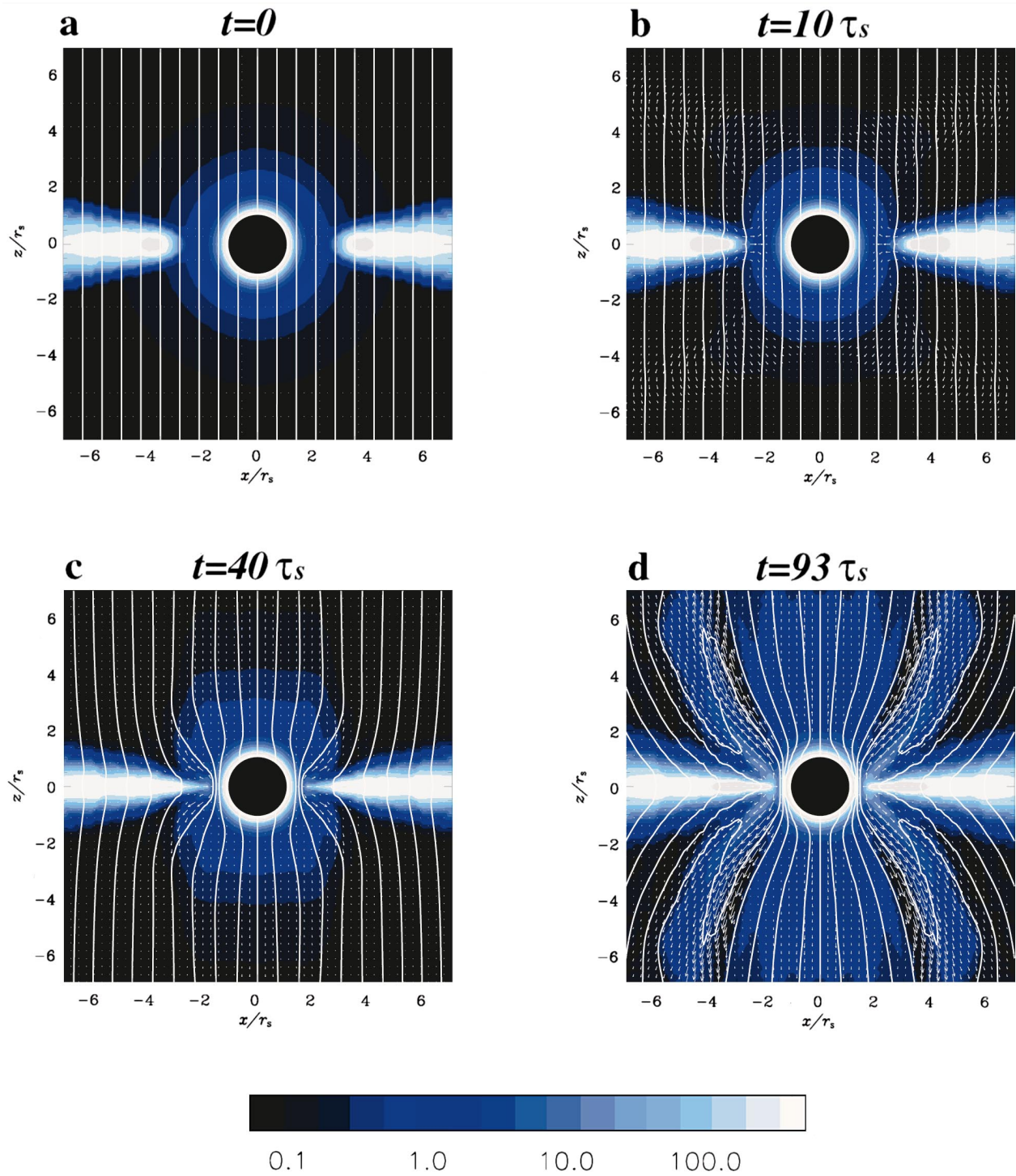


FIG. 1.—Evolution of the jet formation in a black hole magnetosphere. The black circle indicates a black hole (i.e., the region inside the Schwarzschild radius $r \leq r_s$). The solid lines are the magnetic field lines. The blue and white plots show the proper mass density in logarithmic scale. The vector plots show the velocity. A vector with unit length corresponds to light velocity. (a) The initial condition. The coronal plasma is in hydrostatic equilibrium. The accretion disk is rotating around the black hole with Keplerian velocity. The density of the disk is 400 times that of the corona. (b) The rotating disk drags the magnetic field lines, and the large-amplitude, nonlinear Alfvén wave propagates along the magnetic field from the disk. (c) The jet begins to be ejected from the inner edge of the disk. (d) The relativistic jet is formed almost along the magnetic field lines. The maximum poloidal velocity of the jet is $0.88c$, which corresponds to a Lorentz factor of 2.1. The jet has a two-layered structure consisting of the inner fast jet and the outer slow jet. The distance and the time are in units of r_s and $\tau_s \equiv r_s/c$, respectively.

KOIDE, SHIBATA, & KUDOH (see 495, L64)

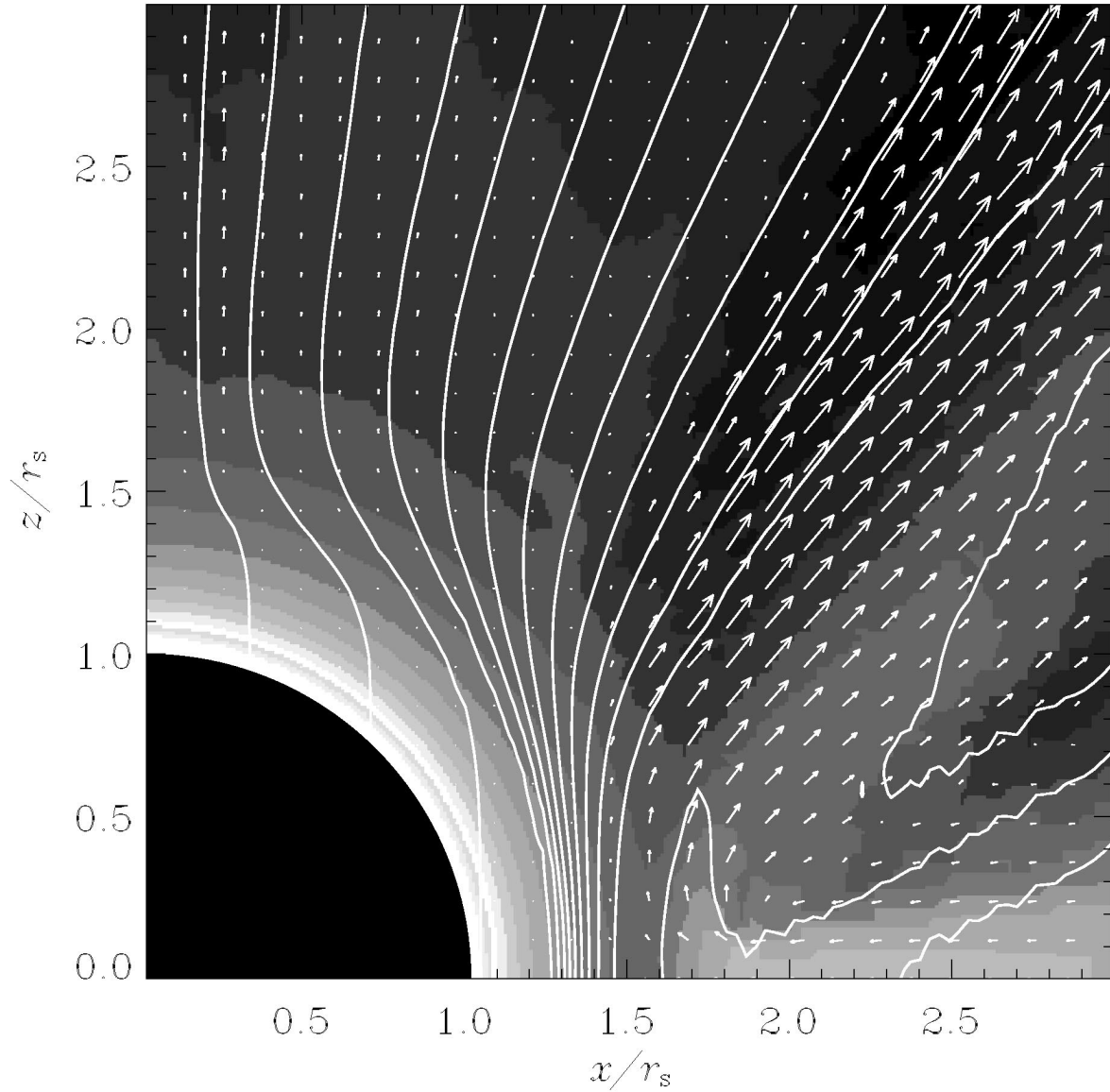


FIG. 2.—Close-up of a snapshot of velocity (*vector*), magnetic field (*solid lines*), and proper mass density (*gray scale*) distributions near the black hole at $t = 91\tau_s$. The black region shows the black hole. We can see both outflow and inflow of the disk plasma.

KOIDE, SHIBATA, & KUDOH (see 495, L64)

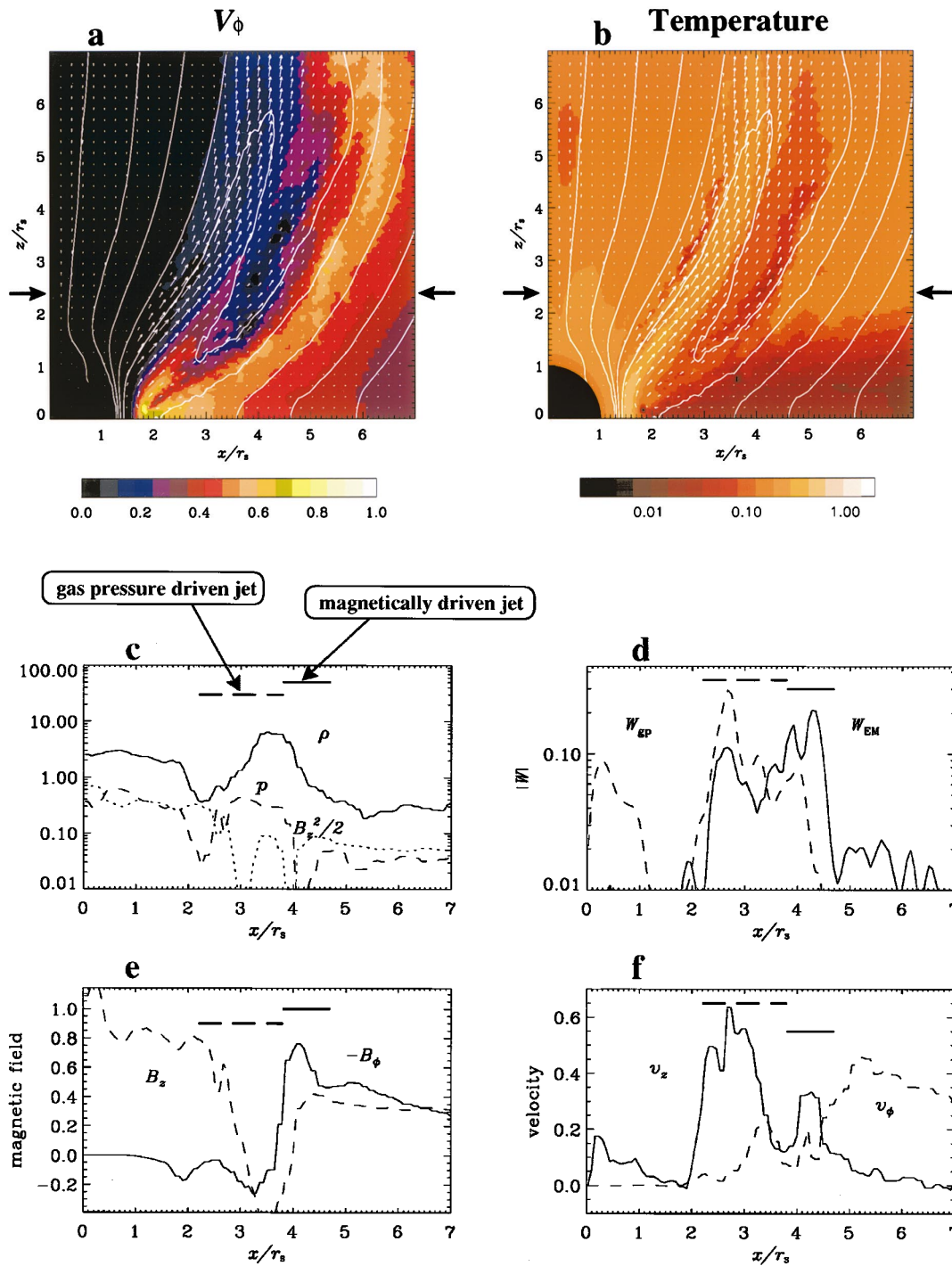


FIG. 3.—(a) Azimuthal component of velocity v_ϕ/c and (b) the temperature $T \equiv p/\rho c^2$ with poloidal velocity (vector plot) and magnetic field (solid lines) at $t = 91\tau_s$. The various physical quantities at $z = 2.4r_s$ [indicated by horizontal arrows beside (a) and (b)] are shown (c–f). Panel (a) shows that the inner fast jet has no azimuthal component of velocity, which indicates that the jet is accelerated by the gas pressure not the magnetic field. On the other hand, the outer jet has finite azimuthal velocity and is accelerated by the magnetic field. (c) The proper mass density ρ , pressure p , and magnetic pressure $B_z^2/2$. (d) The power density W by the gas pressure $W_{gp} \equiv -v \cdot \nabla p$ (dashed lines) and electromagnetic force $W_{EM} \equiv v \cdot \nabla T_{EM}$ (solid lines) to the jet. Here T_{EM} is the Maxwell stress tensor of the electromagnetic field. It is noted that the expressions of W are symbolical but exact, except for the factor of the lapse function. (e) Vertical and azimuthal components of the magnetic field B_z and $-B_\phi$. (f) Vertical and azimuthal components of the velocity: v_z and v_ϕ . The dashed and solid horizontal lines show the regions of the gas pressure–driven jet and the magnetically driven jet, respectively.

KOIDE, SHIBATA, & KUDOH (see 495, L64)

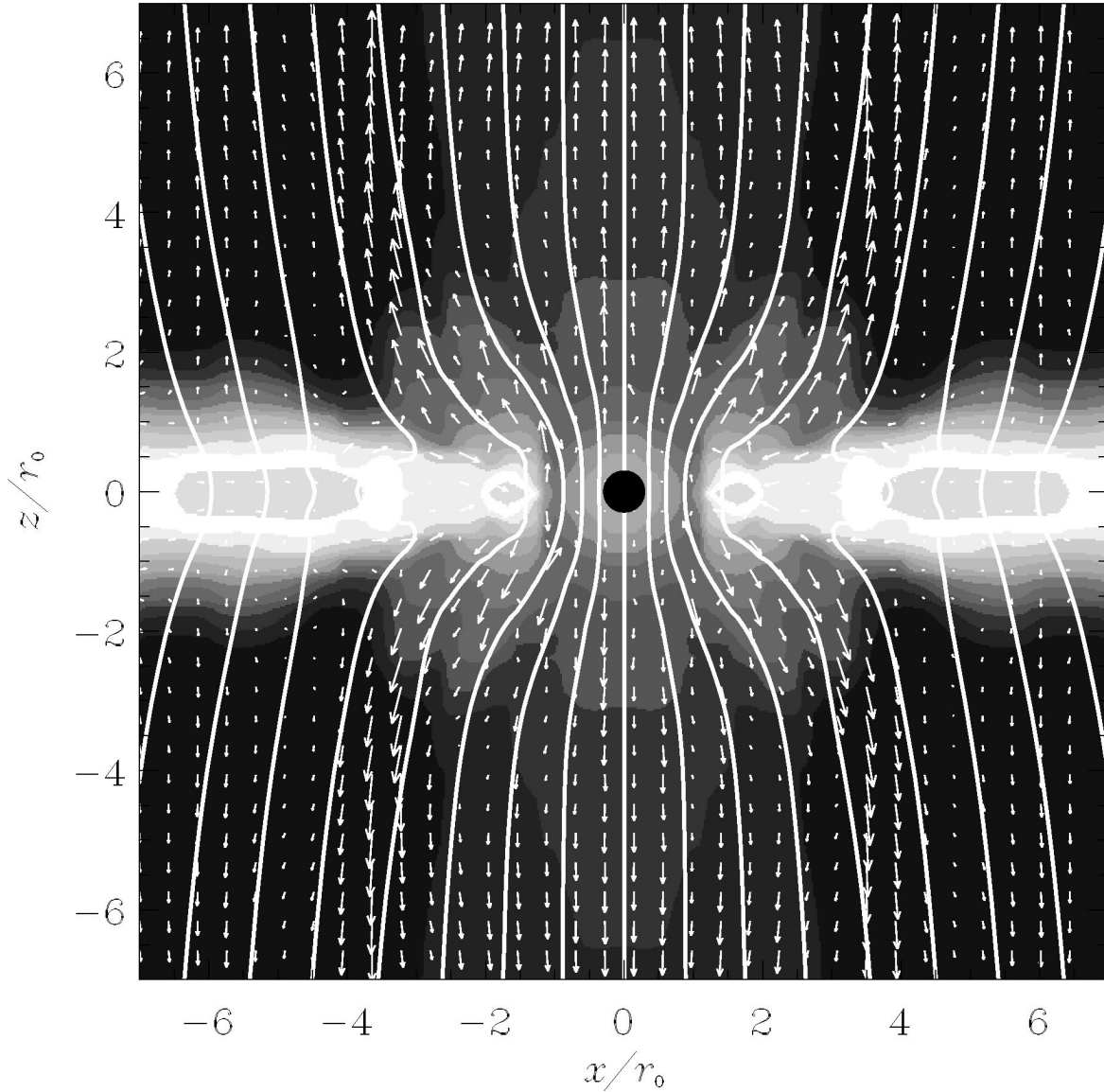


FIG. 4.—The case of the nonrelativistic jet formation at $t = 100\tau_0$, where $\tau_0 \equiv r_0/v_0$, $v_0 = 10^{-2}c$, and $r_0 = r_D/3$, where r_D is the radius of the inner edge of the initial disk. The parameters are the same as those in the relativistic case, except for v_0 . The velocity (*vector*), the rest mass density (*gray scale*), and the magnetic field (*solid lines*) are shown. The scale of the velocity vector normalized by the light velocity of the nonrelativistic case is 1/100 times smaller than that of the relativistic case (Fig. 1d). Around the accretion disk with the Keplerian motion, a magnetically driven jet is formed in the nonrelativistic case. The maximum poloidal component of the velocity is $\sim 0.4V_K$, where V_K is the Keplerian velocity at the inner edge of the initial disk.

KOIDE, SHIBATA, & KUDOH (see 495, L64)